SCIENTIFIC REPORTS

OPEN

SUBJECT AREAS:
ELECTRONIC DEVICES
ELECTRONIC MATERIALS
NANOWIRES

Received
13 June 2014

Accepted
2 October 2014

Published
22 October 2014

Correspondence and requests for materials should be addressed to K.-S.C. (k-s.cho@samsung.com) or S.-W.K. (swkim@ajou.ac.kr)

Diameter-Controlled and Surface-Modified Sb_2Se_3 Nanowires and Their Photodetector Performance

Donghyeuk Choi[1], Yamujin Jang[2], JeeHee Lee[2], Gyoung Hwa Jeong[1], Dongmok Whang[2], Sung Woo Hwang[3], Kyung-Sang Cho[3] & Sang-Wook Kim[1]

[1]Department of Molecular Science and Technology, Ajou University, Suwon, Gyeonggi-do 443-749, South Korea, [2]School of Advanced Materials Science and Engineering, Sungkyunkwan University, Suwon, Gyeonggi-do 440-746, South Korea, [3]Samsung Advanced Institute of Technology(SAIT), Samsung Electronics, 130 Samsung-ro Yeongtong, Suwon, Gyeonggi-do 446-712, South Korea.

Due to its direct and narrow band gap, high chemical stability, and high Seebeck coefficient (1800 μVK^{-1}), antimony selenide (Sb_2Se_3) has many potential applications, such as in photovoltaic devices, thermoelectric devices, and solar cells. However, research on the Sb_2Se_3 materials has been limited by its low electrical conductivity in bulk state. To overcome this challenge, we suggest two kinds of nano-structured materials, namely, the diameter-controlled Sb_2Se_3 nanowires and Ag_2Se-decorated Sb_2Se_3 nanowires. The photocurrent response of diameter-controlled Sb_2Se_3, which depends on electrical conductivity of the material, increases non-linearly with the diameter of the nanowire. The photosensitivity factor ($K = I_{light}/I_{dark}$) of the intrinsic Sb_2Se_3 nanowire with diameter of 80–100 nm is highly improved ($K = 75$). Additionally, the measurement was conducted using a single nanowire under low source-drain voltage. The dark- and photocurrent of the Ag_2Se-decorated Sb_2Se_3 nanowire further increased, as compared to that of the intrinsic Sb_2Se_3 nanowire, to approximately 50 and 7 times, respectively.

Group V-VI binary pnictogen chalcogenide semiconductors, typically crystallizing into a one-dimensional nanostructure in layer-structures parallel to the growth direction, have attracted a lot of attention owing to their specific properties and potential application in various fields, namely, photovoltaic, thermoelectric, and electric devices[1–6]. In particular, antimony selenide (Sb_2Se_3) has promising characteristics, such as narrow band gap (approximately 1 eV), high chemical stability, and high Seebeck coefficient (1800 μVK^{-1}). These properties are attributable to a fast transition from amorphous to crystalline state. Despite its potential in various applications, research on the synthesis and application of the Sb_2Se_3 nanostructures has been limited by challenges, such as its low thermoelectric power factor($\alpha^2\sigma$), low spectral response (R_λ), and low external quantum efficiency(EQE), which result in low electrical conductivity(σ, $10^{-6} \sim 10^{-2}$ $\Omega^{-1}m^{-1}$) in bulk state[5,7–18].

Nonetheless, a few groups have synthesized and studied Sb_2Se_3 nanomaterials to improve its electrical conductivity[19–26]. For example, Golberg *et al.* synthesized single-crystalline Sb_2Se_3 nanowires using a hydrothermal method and investigated its field emission and photoconductive properties. Single crystalline Sb_2Se_3 nanowires, synthesized for 72 h at 180°C exhibited remarkable response to 600 nm of specific visible light with response time of 0.3 sec. However, their time-consuming synthetic process, low electrical conductivity, and low photosensitivity factor ($K = I_{Light}/I_{Dark}$) still hamper practical applications of the Sb_2Se_3 nanowires[22].

Here we suggest new synthetic process of single-crystal Sb_2Se_3 nanowires to overcome these challenges.

Sb_2Se_3 nanowires were synthesized by injection of chemicals into hot solvent (called Hot Injection method). This is one of the most common methods to produce nano-structured materials such as Q-dots, metal alloy nanoparticles, and metal oxide nanoparticles, as size controlled nanoparticles can be easily prepared[27–29]. Using this hot injection method, we could not only produce Sb_2Se_3 nanowires quickly, but could also control the diameter of the nanowires.

Using an additional process, Sb_2Se_3 nanowires decorated with Ag_2Se nanoparticles (Ag_2Se-decorated Sb_2Se_3 nanowires) were also developed. Ag_2Se nanoparticles increased the electrical conductivity and also improved photosensitivity of the Sb_2Se_3 nanowires[30–37].

Results

Characterization of nanowire. Figures 1a shows representative transmission electron microscopy (TEM) image of the intrinsic Sb_2Se_3 nanowires grown using the hot injection method. Individual nanowires had a diameter of

80–100 nm, and a typical length of several micrometers. A high-resolution TEM image and corresponding electron diffraction pattern of the nanowires, as shown in Figure 1(b), revealed that as-synthesized nanowire is single crystal without any detectable crystal defect. The powder X-ray diffraction (XRD) pattern of the intrinsic Sb_2Se_3 nanowires had five prominent peaks, which were indexed to the (120), (230), (221), (240), and (061) planes, corresponding to the orthorhombic crystal structure of Sb_2Se_3 with Pmma space group (Figure 1 c).

Diameter of nanowires is a critical factor, especially in semiconductor nanowires, as their electronic properties strongly depend on diameter of the wire. For instance, GaN nanowires showed various photocurrent responses between 1 nA and 100 μA according to their diameter[38]. In our study, the diameter of Sb_2Se_3 nanowires could be controlled. Figure 2 shows transmission electron microscopy (TEM) and scanning electron microscopy (SEM) images of various diameter of Sb_2Se_3 nanowires, which were controlled by altering the precursor and surfactant ratio. Oleic acid was used as the surfactant in our study. Generally, high concentration of surfactant results in smaller sizes, including diameter, thickness, and length. Three diameter of nanowires were obtained, which were 200–300 nm, 80–100 nm, and 50 nm, with precursor and surfactant ratios of 1 : 2, 1 : 4, and 1 : 20, respectively. An increase in oleic acid resulted in narrow diameter Sb_2Se_3 nanowires. In addition, SEM images, which correlated well with the TEM images, confirmed that the nanowires synthesized had smooth surfaces.

To improve the electrical conductivity of Sb_2Se_3 nanowires, silver precursor ($AgNO_3$) was added to the nanowire solution and nanowires decorated with silver nanoparticles were expected. However, we obtained Ag_2Se-decorated Sb_2Se_3 nanowires. Nonetheless, Ag_2Se-decorated Sb_2Se_3 nanowires were also expected to have better conductivity and photosensitivity than bare Sb_2Se_3 nanowires. Figure 3a clearly shows that each Ag_2Se nanoparticle was incorporated onto the Sb_2Se_3 nanowires. The high-resolution scanning TEM (HR-STEM) image of the Ag_2Se-decorated Sb_2Se_3 nanowires shows that Ag_2Se nanoparticles and Sb_2Se_3 nanowire have different lattice structures and a visible interface (Figure 3b). The HR-STEM image further supports on the synthesis of high crystallinity Ag_2Se nanoparticles and Sb_2Se_3 nanowires. The d spacing is 2.58 Å and 1.98 Å, which is agrees well with the distance of the [121] lattice plane of Ag_2Se and [002] lattice plane of Sb_2Se_3, respectively. Additionally, the unblemished nanowire surface was convincing evidence that selenium of the Ag_2Se nanoparticles originated from excess selenium precursor in the reaction mixture. To confirm the origin of selenium, we removed excess selenium precursor from the reaction mixture and added Ag precursors. We could not obtain the Ag_2Se decorated Sb_2Se_3 nanowires with this reaction condition. The powder X-ray diffraction (XRD) pattern of the Ag_2Se-decorated Sb_2Se_3 nanowires shows that all diffraction patterns can be indexed to the peaks of Ag_2Se(JCPDS 71-2410)and Sb_2Se_3(JCPDS 15-0861) without any visible peak from impurities(Figure 1c).

To find the optimum reaction condition, especially the reaction temperature, the same reaction was conducted at different temperatures. The optimum temperature of the reaction was found to be 100°C. When the temperature was increased above 150°C, the Ag precursor was sufficiently activated to oxidize the as-synthesized Sb_2Se_3 nanowires and resulted in Ag_2Se nanoparticle-decorated Sb_2Se_3 nanowires (150°C, Supporting Information Figures S1a

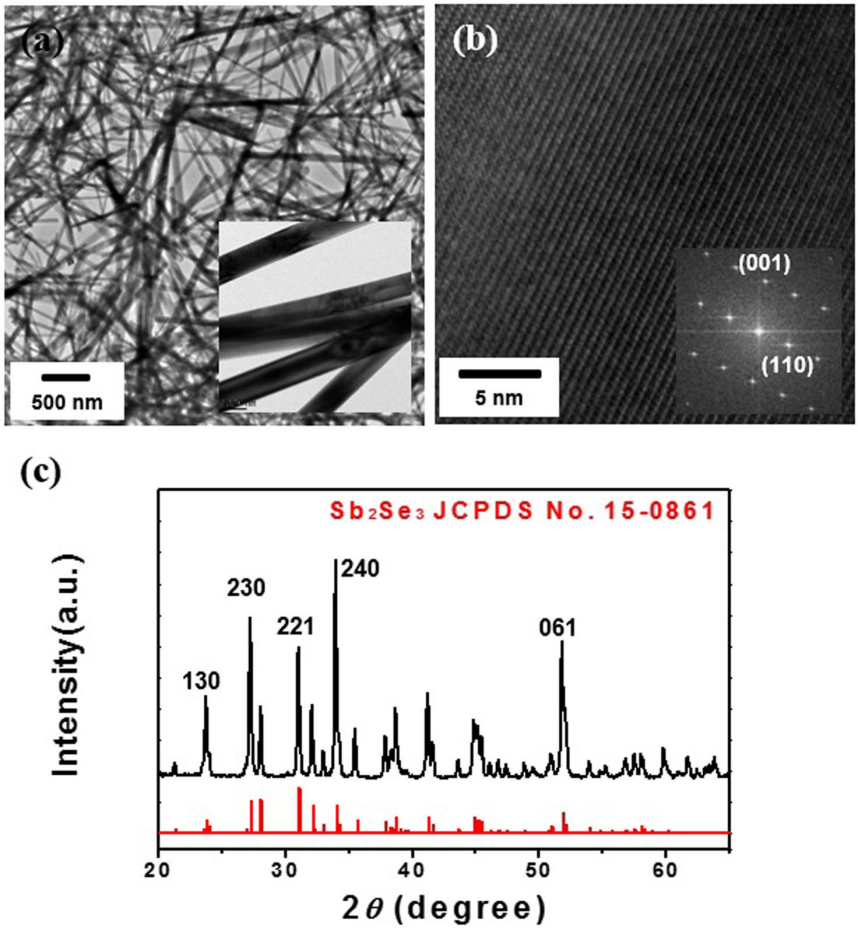

Figure 1 | (a) TEM image of Sb_2Se_3 nanowires; (b) high-resolution TEM images of Figure 1(a) and corresponding SAED pattern; (c) X-ray diffraction patterns of the nanowires.

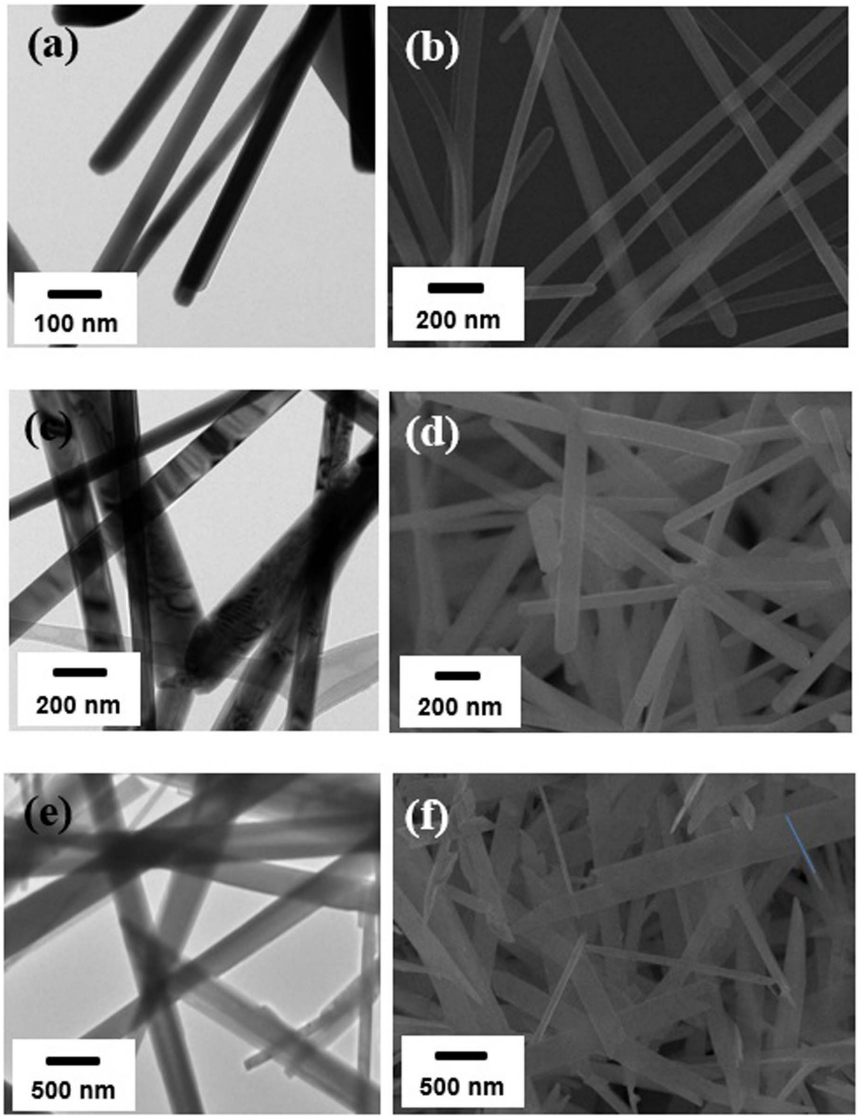

Figure 2 | (a), (c), (e) TEM image of diameter -controlled Sb_2Se_3 nanowires; (b),(d),(f) SEM image of diameter -controlled Sb_2Se_3 nanowires, respectively. Three different nanowire diameter s were obtained, which were 200–300, 80–100, and 50 nm, with precursor and surfactant ratios of 1 : 2, 1 : 4, and 1 : 20, respectively.

and, S1b) and more dissolved nanowires (200°C, Supporting Information Figure S1d and, S1e). The reactivity of the silver precursor decreased at 80°C and no reaction occurred. Extremely high reaction temperature at above 300°C resulted in Ag nanoparticles and a trace of Ag_2Se nanoparticles (Supporting Information Figure S1f and, S1g).

The selenium and silver ratio in the reaction mixture had also a significant effect on the surface morphology of the nanowires. As the amount of Ag increased, more nanoparticles attached to the surface of the nanowires, which then turned coarse. SEM images in Supporting Information Figure S2 show the surface change from bare Sb_2Se_3, 200/1, 100/1, and 50/1 ratios of Se/Ag, respectively.

Interestingly, the size of Ag_2Se nanoparticles on the Sb_2Se_3 nanowires could be also controlled by the diameter of the Sb_2Se_3 nanowires. An increase in the diameter of Sb_2Se_3 nanowires resulted in larger Ag_2Se nanoparticles. The reason was unclear, however, it can be postulated that larger curvature formed from the increase in diameter of the nanowires allowed the Ag_2Se nanoparticles to attach more easily onto the nanowire surface and also allowed for larger sized nanoparticles to be formed. Detailed TEM image of Ag_2Se nanoparticles on nanowire surface can be found in the Supporting Information Figure S3.

In order to investigate the elemental distribution in the Ag_2Se-decorated Sb_2Se_3 nanowires, scanning electron microscopy (SEM) and mapping analysis were performed. SEM mapping images of Se, Ag, and Sb elements are shown in Figure 4. Se atoms were distributed evenly in both, the wire and dot positions. Ag distribution was restricted to the specific areas corresponding to the positions of Ag_2Se nanoparticles on the Sb_2Se_3 nanowires. Ag atoms were found in the nanowire positions, the reason was not clear. EDX-STEM elemental analysis was performed to confirm the results. The O_2-labeled areas in Supporting Information Figure S4, shows that the dot areas were composed of Ag and Se elements, while Sb and Se elements were found in the nanowire region.

Measurement of Photo-device. Photocurrent responses of individual nanowires using 655nm irradiation were measured under ambient conditions at room temperature. Figures 5a and b are the schematic illustration and SEM image, respectively, of a single nanowire device. To fabricate the nanowire device, the nanowires are spin-coated using nanowire/hexane solution and SiO_2/Si substrate, after which, identical parallel electrode patterns with channel length of 4 μm were randomly positioned using the conventional lithography technique. The electrical

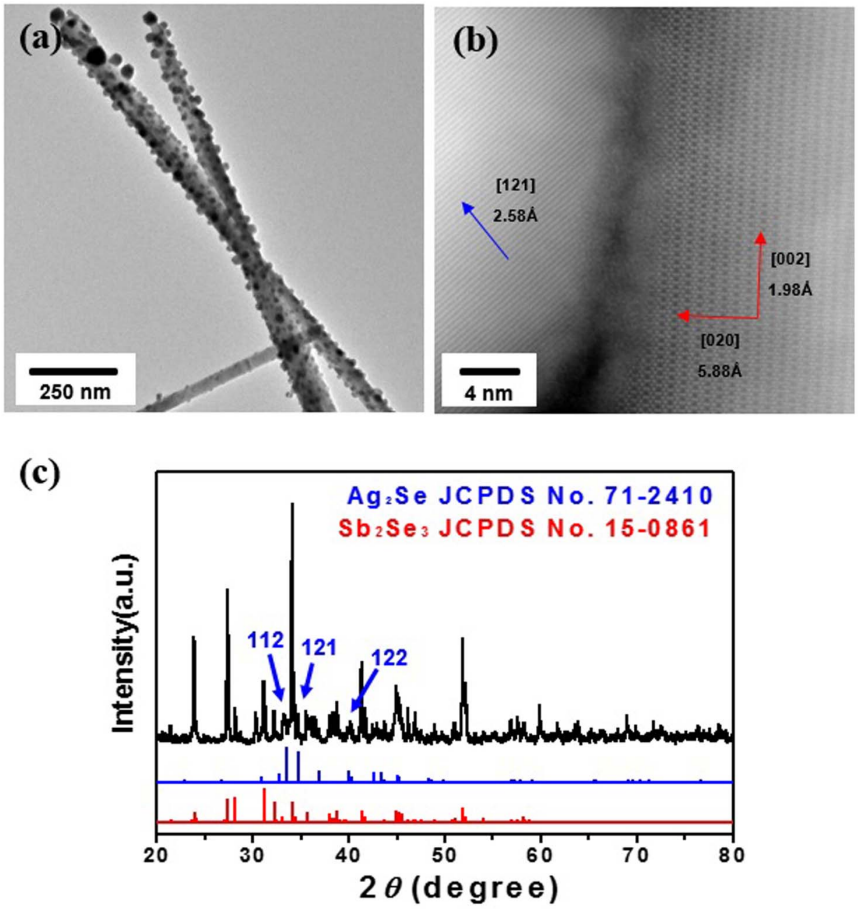

Figure 3 | (a) TEM image of Ag_2Se decorated Sb_2Se_3 nanowires; (b) high-resolution scanning TEM images of Figure 3(a) with the distance between the lattice planes; (c) corresponding X-ray diffraction patterns.

properties were measured either before or after scanning a single nanowire device using SEM.

Figure 5c shows the I–V curves of a single Sb_2Se_3 nanowire device with a diameter of 100 nm measured under dark as well as in presence of 655 nm illumination (15 $mW \cdot cm^{-2}$). Photo-response properties were measured when the light was turned on and off, at 10 sec intervals (Figure 5d). From the I–V curve, the electrical conductivity of the 100 nm diameter Sb_2Se_3 single nanowire in dark condition was $7.6 \times 10^{-2}\Omega^{-1}$ m^{-1} which was similar to the bulk Sb_2Se_3[16,39]. Electrical conductivity of the Sb_2Se_3 nanowire increased under the 655 nm irradiation condition. At 3 V bias, the current under dark conditions was 450 pA, which increased to 34 nA with illumination.

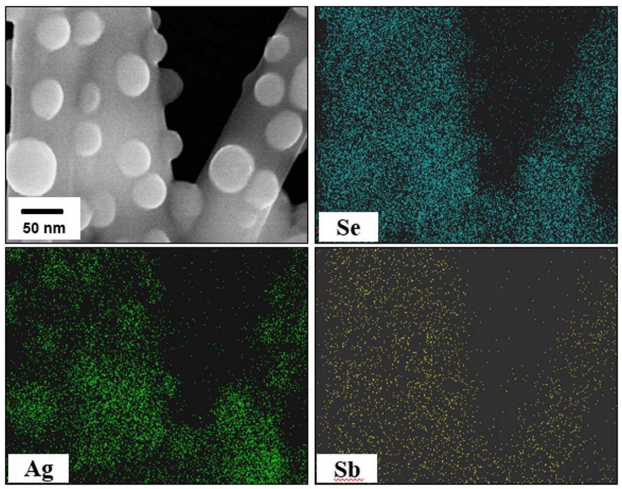

Figure 4 | **SEM image of the Ag_2Se decorated Sb_2Se_3 nanowires and the corresponding EDX mapping images of Se, Ag, and Sb elements, respectively.**

The photosensitivity factor, K was defined as $K = I_{light}/I_{dark}$, where, I_{light} and I_{dark} correspond to current measured with a 655 nm laser turned on and off, respectively. The K factor of the intrinsic Sb_2Se_3 nanowire was found to be 75, which was comparable to previous results[22]. (where K value was 15, with power density of 1.68 $mWcm^{-2}$, under 615 nm illumination). However, the conductivity was 3 times the previous result. The Sb_2Se_3 nanowires used in this study, which were generated using the hot injection method were expected to be more resistant to oxidation and contained fewer surface defects (e.g. dangling bonds) than hydrothermally grown Sb_2Se_3 nanowire due to passivating ligands. Moreover, we used relatively thick (Ti (20 nm)/Au (100 nm)) metal electrodes with very slow deposition rates (1 ~ 2 Å/sec) and a thermal evaporator, which we presumed would allow for better Ohmic contact between the nanowire and the metal electrode.

As shown in Figure 6, time responses of three different diameters of the Sb_2Se_3 nanowire (100 nm, 200 nm, and 400 nm) are also compared. When the Sb_2Se_3 wires are irradiated using same light source (655 nm, 6.5 $mW \cdot cm^{-2}$) photocurrent response increased with the diameter and the ratio of the magnitude of the photocurrent response in 100, 200, and 400 nm wires were 1, 7, and 21, respectively.

The photocurrent in the nanowire for a given photon energy can be expressed as[40]

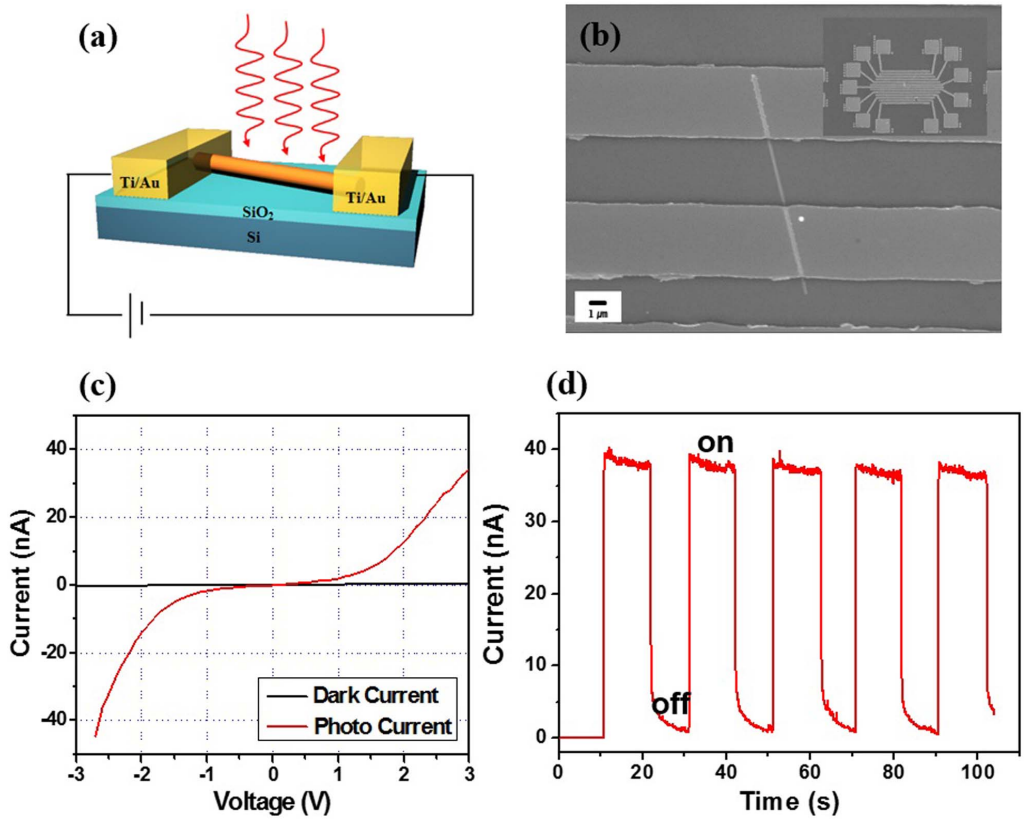

Figure 5 | Photoconductive properties of Sb_2Se_3 nanowires. (a) Schematic illustration and (b) SEM image of single nanowire device. (c) I–V curves of 100 nm diameter Sb_2Se_3 single nanowire in the dark condition and under 655 nm light illumination (15 mW cm^{-2}). (d) Time dependent photocurrent response of Sb_2Se_3 nanowire with the periodic (~10 s) incidence of 655 nm light at an applied voltage of 3 V.

$$I_{PC} = e\frac{P_{abs}}{h\omega}G \quad (1)$$

In addition, the power absorbed in the photoconductor (P_{abs}) and the photoconductive gain (G) can be expressed as

$$P_{abs} = \eta * P_{opt} = \eta * I_0 A \quad (2)$$

$$G = \frac{\tau}{\tau_t} \quad (3)$$

Where, P_{opt} is the incident optical power, I_0 is the illumination intensity, A (=πdl/2) is the exposed surface area of the nanowire, and τ_t is the carrier transit time of the nanowire.

In bulk Sb_2Se_3 material, the increase in photocurrent is proportional to the nanowire surface area (1 : 2 : 4 for 100 nm:200 nm:400 nm) due to light absorption. However, in the Sb_2Se_3 nanowire, the increase in photocurrent was greater than the light absorbed, probably because of the increase in photoconductive gain due to the nanowire structure. In semiconductor nanowires, a depletion space charge layer forms due to the surface state and Fermi-level pinning, which allows for physical separation of the electron and the hole within the nanowire. (Supporting Information Figure S5)[38,40] Until the critical diameter of the nanowire is reached, the depletion layer remains fully depleted and the recombination barrier increases. This may prolong the life of photo-generated carriers and may further increase the photocurrent as the nanowire diameter increases. (Supporting Information Figure S5).

Figures 7a shows the I–V curves of a device fabricated using Ag_2Se-decorated Sb_2Se_3 single nanowire with 100 nm diameter, measured both in dark and under 655 nm illumination (15 mWcm^{-2}). The photo-response property of the Ag_2Se-decorated nanowire was also measured when the light was turned on and off at 10 sec intervals (Figure 7b). Compared with the pure Sb_2Se_3 nanowires of similar size (100 nm diameter) but without Ag_2Se decoration, the current under dark conditions increased approximately 50 times (from 450 pA to 22.8 nA at 3 V) and photocurrent increased approximately 7 times (from 34 nA to 228 nA at 3 V). The K factor of Ag_2Se-decorated Sb_2Se_3 nanowires was 10. The addition of Ag_2Se

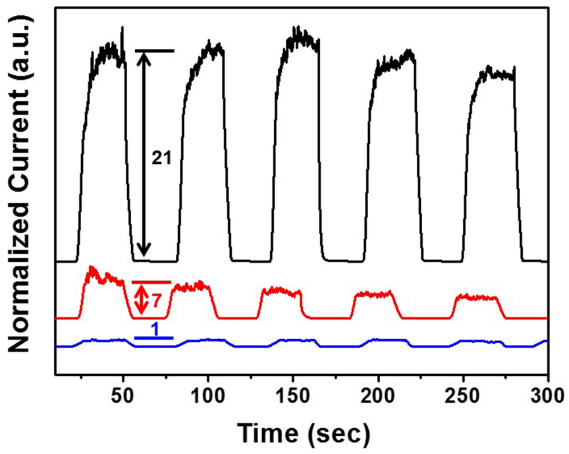

Figure 6 | Time-dependent photocurrent response of the Sb_2Se_3 nanowires with 3 different diameter. (100 nm (blue), 200 nm (red) and 400 nm (black)). Light incidence is 655 nm (5.6 mWcm^{-2}) pulsed light with a period of 30 s. Applied voltage is 3 V.

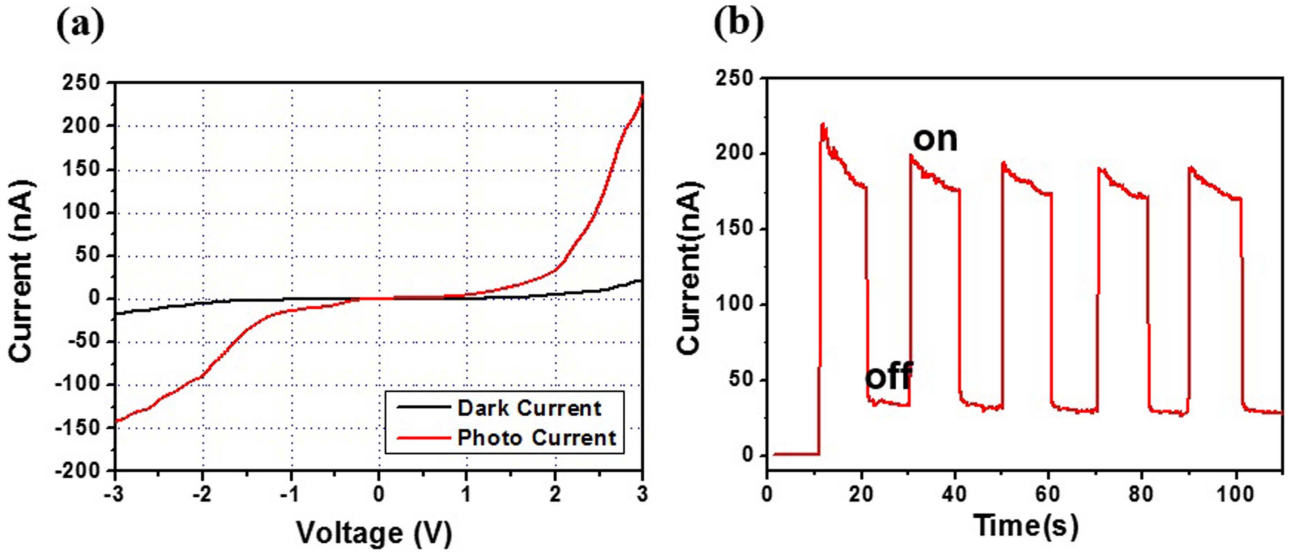

Figure 7 | Photoconductive properties of Ag_2Se decorated Sb_2Se_3 nanowires with 100 nm diameter. (a) I–V curves of single nanowire in the dark condition and under 655 nm light illumination (15 $mWcm^{-2}$). (b) Time dependent photocurrent response nanowire with the periodic (~10 s) incidence of 655 nm light at an applied voltage of 3 V.

decoration to the Sb_2Se_3 nanowire may increase conductivity under dark, due to the decrease in thickness of the depletion layer. The Fermi level of Ag_2Se, a narrow band gap (0.15 eV) semiconductor with properties such as electric conductivity, superionic conductivity, and giant magnetoresistance, is higher than that of Sb_2Se_3 (Supporting Information, Figure S6a)[41,42]. After the Ag_2Se decoration, the electrons from the Ag_2Se particles might flow to the Sb_2Se_3 nanowire surface, thus decreasing the thickness of the depletion layer near the surface due to charge redistribution (Supporting Information Figure S6b). When lights are irradiated, the light absorption efficiency can be increased in the Ag_2Se decorated nanowires by particle induced light scattering[43]. The increase in light absorption and light scattering by Ag_2Se may contribute to photocurrent in addition to the intrinsic photocurrent generated in the Sb_2Se_3 nanowire. The amount of the photocurrent in the decorated nanowire is 10 times than that of the dark current. The K factor of the decorated nanowire is smaller than undecorated nanowire (from 55 to 10) due to the thinner surface depletion layer. The decrease of the degree of surface depletion might increase the intrinsic (dark) conductivity as well as increased the portion of the charge recombination under light irradiation. However, the responsivity ($R_{res} = I_{ph}/I_{irr}$ A, where I_{ph} is the background substituted photocurrent ($I_{illumination}$-I_{dark}) and I_{irr} is the irradiance of the incident light and A is the area of the device) of the Sb_2Se_3 nanowire and Ag_2Se decorated Sb_2Se_3 nanowire are ~560 A/W and ~3400 A/W which is very high and is due to the increased conductivity of our wet-chemically grown Sb_2Se_3 nanowires.

Discussion

In summary, we report the synthesis of diameter-controlled Sb_2Se_3 nanowires by injection of antimony precursor into hot solvent containing selenium precursor as well as production of Ag_2Se-decorated Sb_2Se_3 nanowires, by adding silver precursor ($AgNO_3$) to the nanowire solution. The presence of Ag_2Se nanoparticles on the nanowires was confirmed using TEM, XRD, SEM mapping, and EDX-STEM elemental analysis. Photocurrent response of individual nanowires using 655 nm light irradiation was measured under ambient conditions at room temperature. The photo-device comprising of 100 nm Sb_2Se_3 nanowire had an electrical conductivity of approximately 7.6 $\times 10^{-2}\ \Omega^{-1}\ m^{-1}$ in dark conditions and K factor of 75. The current obtained in dark conditions was 450 pA, which increased to 34 nA with light. In addition, as the diameter of the Sb_2Se_3 nanowire increased, the photocurrent increased non-linearly. Under identical conditions, the photo-device comprising of Ag_2Se-decorated 100 nm Sb_2Se_3 nanowires had a 50-fold increase in dark current from 450 pA to 22.8 nA, and 7-fold increase of photocurrent from 34 nA to 228 nA in comparison to bare Sb_2Se_3 nanowires.

Methods

Materials. Selenium metal powder was purchased from Strem Chemical Inc. Oleic acid, 1-octadecene, and silver nitrate were purchased from Sigma-Aldrich. All chemicals were used without further purification.

Synthesis of intrinsic Sb_2Se_3 nanowires. Selenium metal (0.3 mmol, 24 mg), oleic acid (0.9 mmol, 256 mg), and 10 ml of 1-octadecene were added into a 50 ml three-neck flask, and the mixture was degassed under vacuum at 100°C for 1h. To prepare antimony precursor solution, 0.3 mmol of antimony chloride (68 mg, Aldrich), 0.9 mmol of stearic acid (256 mg, Aldrich), and 4 ml of 1-octadecene (Aldrich) in another flask were degassed at room temperature for 1 h, and purged with nitrogen. The antimony precursor solution was quickly injected into the selenium and surfactant solution at 250°C under nitrogen atmosphere, the mixture was stirred at the same temperature for 10 min, and then cooled to room temperature. Sb_2Se_3 nanowires were precipitated from the reaction by adding ethanol and separated by centrifugation.

Synthesis of Ag_2Se decorated Sb_2Se_3 nanowires. To attach Ag_2Se nanoparticles onto the surface of Sb_2Se_3 nanowires, 3 μmol of silver nitrate (0.51 μg, Aldrich) was added into the above Sb_2Se_3 nanowires solution at room temperature. Subsequently, the temperature was raised to 100°C, the mixture was stirred at this temperature for 90 min under nitrogen atmosphere, and then cooled to room temperature. Sb_2Se_3 nanowires with Ag_2Se nanoparticles attached were precipitated from the reaction by adding ethanol and separated by centrifugation.

Photo-device fabrication. Photodevices were fabricated from bare Sb_2Se_3 nanowires as well as Ag_2Se-decorated Sb_2Se_3 nanowires. Nanowires dispersed in hexane were spread on the SiO_2 (100 nm)/Si wafer and then O_2 plasma ashing proceed by Reactive Ion Etching(RIE) to remove residual organic species. Photolithography and thermal evaporation techniques were used to deposit the Ti (20 nm)/Au (100 nm) electrodes in contact with the individual nanowires. The channel length of the photodevice was 4 μm. I–V and photoswitching are measured with a 655 nm laser (15 $mWcm^{-2}$) at room temperature under air.

Characterization. The nanowires dispersed in hexane were spread on a copper grid and a silicon wafer for measurement using transmission electron microscopy (TEM) and scanning electron microscopy (SEM), respectively. TEM image and STEM-EDX were taken with a FEI Tecnai G2 F30 Super-Twin transmission electron microscope operating at 300 kV. SEM image and X-ray mapping data were obtained with a JSM-6700F field emission scanning electron microscope at 30 kV operating voltage, equipped with an INCA energy dispersive X-ray spectrometer (EDS). X-ray diffraction (XRD) patterns were taken using a Rigaku Ultima III diffractometer

equipped with a rotating anode and Cu K_α radiation source ($\lambda = 0.15418$ nm). Electrical characterization of the nanowire devices was performed using a probe station (MSTECH MST-6000C, Korea) and the Keithley SCS-4200 system.

1. Rodríguez-Lazcano, Y., Peña, Y., Nair, M. T. S. & Nair, P. K. Polycrystalline thin films of antimony selenide via chemical bath deposition and post deposition treatments. *Thin Solid Films* **493**, 77–82 (2005).
2. Guijarro, N. *et al.* Toward Antimony Selenide Sensitized Solar Cells: Efficient Charge Photogeneration at spiro-OMeTAD/Sb_2Se_3/Metal Oxide Heterojunctions. *J. Phys. Chem. Lett.* **3**, 1351–1356 (2012).
3. Dresselhaus, M. S. *et al.* New Directions for Low-Dimensional Thermoelectric Materials. *Adv. Mater.* **19**, 1043–1053 (2007).
4. Fernández, A. M. & Merino, M. G. Preparation and characterization of Sb_2Se_3 thin films prepared by electrodeposition for photovoltaic applications. *Thin Solid Films* **366**, 202–206 (2000).
5. Vomiero, A. *et al.* One-dimensional nanostructured oxides for thermoelectric applications and excitonic solar cells. *Nano Energy* **1**, 372–390 (2012).
6. Yan, C. & Lee, P. S. Recent Progresses in Improving Nanowire Photodetector Performances. *Sci. Adv. Mater.* **4**, 241–253 (2012).
7. Iovu, M. S., Colomeico, E. P. & Vasiliev, I. A. Photoconductivity of Amorphous Sb_2Se_3 and Sb_2Se_3:Sn Thin Films. *CHALCOGENIDE LETT.* **4**, 109–113 (2007).
8. Yu, Y., Wang, R. H., Chen, Q. & Peng, L. M. High-Quality Ultralong Sb_2Se_3 and Sb_2S_3 Nanoribbons on a Large Scale via a Simple Chemical Route. *J. Phys. Chem. B* **110**, 13415–13419 (2006).
9. Mehta, R. J. *et al.* High Electrical Conductivity Antimony Selenide Nanocrystals and Assemblies. *Nano Lett.* **10**, 4417–4422 (2010).
10. Hurych, Z., Davis, D., Buczek, D. & Wood, C. Photoemission studies of crystalline and amorphous Sb_2Se_3. *Phys. Rev. B* **9**, 4392–4404 (1974).
11. Zhai, T. *et al.* Single-Crystalline Sb_2Se_3 Nanowires for High-Performance Field Emitters and Photodetectors. *Adv. Mater.* **22**, 4530–4533 (2010).
12. Bacewicz, R. & Ciszek, T. F. Liquid encapsulated crystal growth and electrical properties of Sb_2Se_3 and Bi_2S_3. *J. Cryst. Growth* **109**, 133–136 (1991).
13. Gilbert, L. R., Van Pelt, B. & Wood, C. The Thermal Activation Energy of Crystalline Sb_2Se_3. *J. Phys. Chem. Solids* **35**, 1629–1632 (1974).
14. Deng, Z., Mansuripur, M. & Muscat, A. J. Simple Colloidal Synthesis of Single-Crystal Sb-Se-S Nanotubes with Composition Dependent Band-Gap Energy in the Near-Infrared. *Nano Lett.* **9**, 2015–2020 (2009).
15. Vadapoo, R., Krishnan, S., Yilmaz, H. & Marin, C. Electronic structure of antimony selenide(Sb_2Se_3) from GW calculations. *phys. status solidi B* **248**, 700–705 (2011).
16. Chakraborty, B. R., Ray, B., Bhattacharya, R. & Dutta, A. K. Magnetic and Electric Properties of Antimony Selenide(Sb_2Se_3) Crystals. *J. Phys. Chem. Solids* **41**, 913–917 (1980).
17. Wood, C., Hurych, Z. & Shaffer, J. C. Optical and Transport Properties of Amorphous Sb_2Se_3. *J. Non-Cryst. Solids.* **8–10**, 209–214 (1972).
18. Abd El-Salam, F., Afifi, M. A. & Abd El-Wahabb, E. Electrical resistivity of crystalline Sb_2Se_3. *Vacuum* **44**, 111–116 (1993).
19. Chang, H.-W., Sarkar, B. & Liu, C. W. Synthesis of Sb_2Se_3 Nanowires via a Solvothermal Route from the Single Source Precursor $Sb[Se_2P(O^iPr)_2]_3$. *Cryst. Growth Des.* **7**, 2691–2695 (2007).
20. Ma, J. *et al.* Controlled Synthesis of One-Dimensional Sb_2Se_3 Nanostructures and Their Electrochemical Properties. *J. Phys. Chem. C* **113**, 13588–13592 (2009).
21. Chen, M. & Gao, L. Polyol method synthesis and characterization of nanoscale Sb_2Se_3 wires. *Mater. Res. Bull.* **40**, 1120–1125 (2005).
22. Zhai, T. *et al.* Recent Developments in One-Dimensional Inorganic Nanostructures for Photodetectors. *Adv. Funct. Mater.* **20**, 4233–4248 (2010).
23. Chen, G. *et al.* The Fractal Splitting Growth of Sb_2S_3 and Sb_2Se_3 Hierarchical Nanostructures. *J. Phys. Chem. C* **112**, 672–679 (2008).
24. Zhou, B. & Zhu, J.-J. Microwave-assisted synthesis of Sb_2Se_3 submicron rods, compared with those of Bi_2Te_3 and Sb_2Te_3. *Nanotechnology* **20**, 085604 (2009).
25. Ma, J. *et al.* One-dimensional Sb_2Se_3 nanostructures: solvothermal synthesis, growth mechanism, optical and electrochemical properties. *CrystEngComm* **13**, 2369–2374 (2011).
26. Yang, R. B. *et al.* Pulsed Vapor-Liquid-Solid Growth of Antimony Selenide and Antimony Sulfide Nanowires. *Adv. Mater.* **21**, 3170–3174 (2009).
27. Murray, C. B., Norris, D. J. & Bawendi, M. G. Synthesis and characterization of nearly monodisperse CdE (E = sulfur, selenium, tellurium) semiconductor nanocrystallites. *J. Am. Chem. Soc.* **115**, 8706–8715 (1993).
28. Sun, S. *et al.* Monodisperse FePt nanoparticles and ferromagnetic FePt nanocrystal superlattices. *Science* **287**, 1989–1992 (2000).
29. Hyeon, T. *et al.* Synthesis of Highly Crystalline and Monodisperse Maghemite Nanocrystallites without a Size-Selection Process. *J. Am. Chem. Soc.* **123**, 12798–12801 (2001).
30. Liu, K., Sakurai, M., Liao, M. & Aono, M. Giant Improvement of the Performance of ZnO Nanowire Photodetectors by Au Nanoparticles. *J. Phys. Chem. C* **114**, 19835–19839 (2010).
31. Lin, D., Wu, H., Zhang, R. & Pan, W. Enhanced Photocatalysis of Electrospun Ag-ZnO Heterostructured Nanofibers. *Chem. Mater.* **21**, 3479–3484 (2009).
32. Zheng, Y. *et al.* Photocatalytic Activity of Ag/ZnO Heterostructure Nanocatalyst: Correlation between Structure and Property. *J. Phys. Chem. C* **112**, 10773–10777 (2008).
33. Lin, D. *et al.* Enhanced UV photoresponse from heterostructured Ag-ZnO nanowires. *Appl. Phys. Lett.* **94**, 172103 (2009).
34. He, J. H. *et al.* Large-Scale Ni-Doped ZnO Nanowire Arrays and Electrical and Optical Properties. *J. Am. Chem. Soc.* **127**, 16376–16377 (2005).
35. Prabhakar, R. R. *et al.* Efficient multispectral photodetection using Mn doped ZnO nanowires. *J. Mater. Chem.* **22**, 9678–9683 (2012).
36. Kouklin, N. Cu-Doped ZnO Nanowires for Efficient and Multispectral Photodetection Applications. *Adv. Mater.* **20**, 2190–2194 (2008).
37. Zheng, Y. *et al.* Ag/ZnO Heterostructure Nanocrystals: Synthesis, Characterization, and Photocatalysis. *Inorg. Chem.* **46**, 6980–6986 (2007).
38. Calarco, R. *et al.* Size-dependent Photoconductivity in MBE-Grown GaN-Nanowires. *Nano Lett.* **5**, 981–984 (2005).
39. Zheng, X. *et al.* Growth of Sb_2E_3 (E = S, Se) Polygonal Tubular Crystals via a Novel Solvent-Relief-Self-Seeding Process. *Inorg. Chem.* **41**, 455–461 (2002).
40. Soci, C. *et al.* Nanowire Photodetectors. *J. Nanosci. Nanotechnol.* **10**, 1430–1449 (2010).
41. Gates, B. *et al.* Single-Crystalline Nanowires of Ag_2Se Can Be Synthesized by Templating against Nanowires of Trigonal Se. *J. Am. Chem. Soc.* **123**, 11500–11501 (2001).
42. Sahu, A. *et al.* Solid-Phase Flexibility in Ag_2Se Semiconductor Nanocrystals. *Nano Lett.* **14**, 115–121 (2013).
43. Atwater, H. A. & Polman, A. Plasmonics for improved photovoltaic devices. *Nature Mat.* **9**, 205–213 (2010).

Acknowledgments

This work was supported by the New & Renewable Energy Core Technology Program of KETEP (No. 201330300001), Basic Science Research Program through the National Research Foundation of Korea(NRF) funded by the Ministry of Science, ICT & Future Planning(No. 2014R1A5A1009799) and the Priority Research Centers Program (2012-0006687), Republic of Korea. We thank J. Lee for TEM analysis.

Author contributions

All authors contributed to the design of the experiments. D.C., K-S.C. and S-W.K. conceived and designed this study. D.C. synthesized nanowires. Y.J., J.L. fabricated photo-device. G.H.J. and S.W.H. analyzed data. D.W. advised experiment. D.W., K-S.C. and S-W.K. wrote the paper.

Additional information

Supplementary information accompanies this paper at http://www.nature.com/scientificreports

Competing financial interests: The authors declare no competing financial interests.

How to cite this article: Choi, D. *et al.* Diameter-Controlled and Surface-Modified Sb_2Se_3 Nanowires and Their Photodetector Performance. *Sci. Rep.* **4**, 6714; DOI:10.1038/srep06714 (2014).